Journal of Inflammation Research

Dovepress
Taylor & Francis Group

Open Access Full Text Article

ORIGINAL RESEARCH

The Interplay Among Gut Microbial Composition, Short-Chain Fatty Acid Metabolism and Gut-Kidney Oxidative Stress: Correlation with Diarrhea

Junxi Shen[1,2], Leyao Fang[1,2], Xinxin Peng[2,3], Miao Jiang[1,2], Xuejiao Xie[1,2], Zhoujin Tan[1,2]

[1]School of Traditional Chinese Medicine, Hunan University of Chinese Medicine, Changsha, Hunan, People's Republic of China; [2]Hunan Key Laboratory of Traditional Chinese Medicine Prescription and Syndromes Translational Medicine, Changsha, Hunan, People's Republic of China; [3]The First Hospital of Hunan University of Chinese Medicine, Changsha, Hunan, People's Republic of China

Correspondence: Zhoujin Tan; Xuejiao Xie, Email tanzhjin@sohu.com; xuejiao123@hnucm.edu.cn

Background: Gut microbiota dysbiosis in the colon, leading to gut-kidney inflammatory responses, is a key cause of exacerbated diarrhea. The upstream mechanistic relationship between colonic microecological disturbance and gut-kidney interaction injury remains unclear.

Methods: In this study, a total of 20 KM mice were used. We established a mouse diarrhea model, analyzed colonic microbiota composition via 16S rRNA sequencing, quantified short-chain fatty acids (SCFAs) using gas chromatography-mass spectrometry (GC-MS), and measured sirtuin 3 (SIRT3), superoxide dismutase 2 (SOD2) protein levels, total SOD activity, and ROS levels in colonic and kidney tissues. Mouse physiological signs and histopathological changes were also evaluated.

Results: In model mice, the relative expression levels of SIRT3 and SOD2 proteins in colon and kidney tissues were significantly decreased ($P < 0.01$). Similarly, the SOD enzyme activity also showed a significant reduction, with $P < 0.05$ in the colon and $P < 0.01$ in the kidney. In contrast, the intensity of ROS was significantly increased ($P < 0.01$). Colonic microbial diversity declined. *Streptococcus* showed a significant enrichment in the colon ($P < 0.01$), and the contents of propionic acid and isobutyric acid were significantly decreased ($P < 0.05$). A negative correlation was observed between the abundance of *Streptococcus* and SCFAs, and there were correlations between the abundance of *Streptococcus* and SOD enzyme activity in tissues as well as ROS intensity.

Conclusion: Therefore, we infer that there are associations between gut microbiota dysbiosis in the colon, altered levels of SCFAs, exacerbated gut-kidney oxidative stress responses, and the onset and progression of diarrhea.

Keywords: gut microbiota, SCFAs, oxidative stress, gut-kidney interaction, diarrhea

Introduction

The microbial community in the human gut represents a complex consortium, comprising over 100 trillion microbial cells that encompass more than 1000 distinct species.[1] Gut microbiota facilitate the breakdown of indigestible plant polysaccharides and resistant starches, thereby promoting the absorption of complex carbohydrates.[2] Through dietary fiber degradation, this microbial community generates organic acids, gases, and substantial quantities of short-chain fatty acids (SCFAs), with acetate, propionate, and butyrate being the predominant SCFAs produced.[3] The total concentration of SCFAs can reach 50–150 mM in the colon, where microbial biomass is highest.[4] SCFAs influence host intestinal epithelial cell proliferation and differentiation while modulating intestinal endocrine function, host immune responses, and barrier integrity.[5] Gut microbiota dysbiosis diminishes the production of microbiota-derived antioxidants (eg, SCFAs), leading to excessive reactive oxygen species (ROS) generation and disruption of the host's antioxidant defense system.[6] Under disease conditions, defects in the colonic barrier can lead to intestinal microbial translocation, exacerbating the damage caused by oxidative stress in the gut-kidney crosstalk.[7] Recent advances in understanding the gut-kidney axis have elucidated critical interactions between gut microbiota, their metabolites, and intestinal/renal functions, revealing their pivotal role in maintaining intestinal and renal health through mediation of immune tolerance, oxidative stress, and metabolic processes.[8,9]

https://doi.org/10.2147/JIR.S588857
Received: 30 December 2025
Accepted: 1 April 2026
Published: 20 April 2026

SIRT3 is a nicotinamide adenine dinucleotide (NAD^+)-dependent mitochondrial protein deacetylase that regulates superoxide dismutase 2 (SOD2) activity by removing acetyl modifications from proteins, thereby maintaining normal cellular physiological functions.[10,11] SOD2, a manganese superoxide dismutase, plays a critical role in modulating superoxide byproducts generated during oxidative phosphorylation, mitigating ROS overproduction and preserving intracellular redox homeostasis.[12] While ROS function as signaling molecules involved in cellular signal transduction, proliferation, and immune defense, excessive ROS accumulation triggers inflammasome-mediated inflammatory cascades, leading to cellular damage and death.[13] Under SIRT3 deficiency, organisms exhibit reduced oxygen consumption and elevated ROS levels;[14] conversely, SIRT3 overexpression attenuates mitochondrial damage, tubular epithelial cell apoptosis, and accumulation of pro-inflammatory cytokines and oxidative stress in animal models of acute kidney injury.[15] The gut microbiota and its metabolites modulate systemic SIRT3, SOD2, and ROS levels to suppress oxidative stress, thereby reducing histopathological damage and inflammatory responses.[16–18] These findings underscore the physiological and pathological interplay between gut microbiota regulation of the SIRT3-SOD2-ROS signaling pathway and the gut-kidney axis.

In our previous research, by inducing intestinal dysbiosis through a combination of antibiotics, we demonstrated that intestinal dysbiosis serves as a crucial mediator in the gut-kidney interaction injury observed in diarrhea model mice. NLRP3 inflammasome-related molecules and inflammatory cytokines are involved in this pathophysiological process.[19] The SIRT3-SOD2-ROS pathway functions as an upstream signaling cascade of the NLRP3 inflammasome.[12] Gut microbiota dysbiosis and abnormalities in the synthesis and metabolism of SCFAs result in oxidative stress responses in the body. Therefore, building upon our prior studies, we will replicate the diarrhea mouse model to investigate the correlations among gut microbiota composition, intestinal SCFAs, molecules related to the SIRT3-SOD2-ROS pathway in colonic and renal tissues, and diarrhea. We aim to clarify the impact of intestinal microecological dysregulation on molecules related to the SIRT3-SOD2-ROS pathway and its underlying mechanisms in renal-associated diarrhea. In particular, this study attempts to systematically link colonic microbiota, SCFAs, and molecules related to the SIRT3-SOD2-ROS pathway, thereby providing further evidence that intestinal microecological dysregulation is a key factor in aggravating diarrhea.

Materials and Methods

Experimental Animals and Housing Environment

All animal experiments complied with ARRIVE guidelines. Approval for this research has been granted by the Institutional Animal Care and Usage Committee of Hunan University of Chinese Medicine, with the ethics approval number being HNUCM21-2409-14. 20 specific pathogen free (SPF) male Kunming mice, weighing approximately 20 ±2g, were purchased from Hunan Slaccas Jingda Laboratory Animal Co., Ltd. The animal license number is [SCXK (Xiang) 2019–0004]. These mice were raised in the SPF-grade breeding environment of the Experimental Animal Center at Hunan University of Chinese Medicine. The temperature was controlled at (22±2)°C, the humidity at around 50%, and the light/dark cycle was set to 12 hours. During the experimental period, the mice had free access to standard chow and water, both of which were uniformly supplied by the Experimental Animal Center of Hunan University of Chinese Medicine. To exclude the influence of sex on the gut microbiota,[20] mice of a single sex were used in this study.

Reagents and Reagent Kits

Adenine (purchased from Biofroxx, Germany, Cat. No.: 1163GR005), *Folium sennae* (obtained from Bozhou Huqiao Pharmaceutical Co., Ltd., Lot NO.: 2,311,300,022), Reactive Oxygen Species (ROS) Fluorescence Assay Kit (provided by Jiangsu Aidisheng Biotechnology Co., Ltd., Cat. No.: ADS-W-HY009), Superoxide Dismutase (SOD) Assay Kit (using the WST-8 method, from Jiangsu Aidisheng Biotechnology Co., Ltd., Cat. No.: ADS-W-KY011), Beta Actin Monoclonal Antibody (purchased from Wuhan Sanying Biotechnology, Inc., Cat. No.: 66,009-1-Ig), SIRT3 Polyclonal Antibody (from Wuhan Sanying Biotechnology, Inc, Cat. No.: 10,099-1-AP), SOD2 Polyclonal Antibody (from Wuhan Sanying Biotechnology, Inc., Cat. No.: 24,127-1-AP), HRP-labeled Goat Anti-Mouse Secondary Antibody (purchased

from Wuhan Boster Biological Engineering Co., Ltd., Cat. No.: BA1051), and HRP-labeled Goat Anti-Rabbit Secondary Antibody (from Wuhan Boster Biological Engineering Co., Ltd., Cat. No.: BA1054).

Drug Preparation

Preparation of adenine suspension:[21] Adenine was dissolved in sterile purified water to achieve a final concentration of 5 $mg \cdot mL^{-1}$ for administration. The suspension was prepared freshly and shaken well immediately before use. Preparation of *Folium sennae* decoction:[22] *Folium sennae* was placed in a beaker, soaked in distilled water for 30 min, and then subjected to a 75 °C water bath for 30 min. The resulting solution was filtered to collect the filtrate, which was subsequently concentrated at 75 °C to achieve a crude drug concentration of 1 $g \cdot mL^{-1}$. The prepared *Folium sennae* decoction was stored at 4 °C for future use.

Animal Grouping and Intervention

After adaptive feeding, 20 mice were randomly divided into a normal group (CC) and a diarrhea model group (CM), with 10 mice in each group. In line with the established practices from the team's previous research,[23] we adopted a consistent approach regarding the number of mice in each group and the method for establishing the diarrhea model. From day 1 to day 14 of modeling, the CM group received intragastric administration of an adenine suspension (50 $mg \cdot kg^{-1}$) once daily. From day 8 to day 14, the CM group was also administered a *Folium sennae* decoction (10 $g \cdot kg^{-1}$) via intragastric gavage once daily. Meanwhile, the CC group received an equal volume of sterile water via intragastric gavage for 14 consecutive days.

General Sign Observation

The mental state, spontaneous activity, fecal morphology and color, and perianal cleanliness of mice in each group were observed. On the 14th day of model establishment, fecal samples were collected from the mice, rectal temperatures were measured, and body weights were recorded. The wet weight of the fecal samples was weighed and recorded. Subsequently, the samples were dried to a constant weight at 110 °C, and the dry weight was recorded. The fecal moisture content was then calculated.[24,25]

Sample Collection

The sample collection methods were conducted with reference to previously established protocols.[26–28] On the 15th day of the experiment, Zoletil® 50 (Tiletamine/Zolazepam, 50 $mg \cdot kg^{-1}$) was intraperitoneally injected into the mice for anesthesia, followed by blood sample collection. Subsequently, euthanasia was promptly and swiftly carried out on the animals using the cervical dislocation method to minimize animal suffering to the greatest extent. After that, the mice were dissected, and renal tissues were collected and preserved. Sterile instruments were used to collect colonic contents. Then, the colon was longitudinally incised with surgical scissors, thoroughly rinsed with normal saline, and stored. The kidney and colon tissues used for preparing pathological sections were preserved in paraformaldehyde, while the remaining samples were stored at −80 °C.

Observation of Histomorphology in Colon and Kidney Samples

The colon and kidney tissues were fixed with 4% paraformaldehyde, dehydrated through a graded ethanol series, embedded in paraffin, sectioned, and stained with hematoxylin-eosin (HE). Following gradient dehydration, the sections were mounted with neutral resin and examined for pathological changes under an optical microscope.

Detection of SIRT3 and SOD2 Protein Levels in Colon and Kidney Tissues by Western Blot

Total protein was extracted from mouse colon and kidney tissues, mixed with loading buffer, and denatured by boiling for 10 min. The samples were then stored at −20 °C for subsequent use. Following this, gel loading, electrophoresis, membrane transfer, and blocking procedures were performed. PVDF membranes were incubated overnight at 4 °C with primary antibodies (SIRT3, SOD2, and β-Actin) and subsequently washed. After incubation with HRP-conjugated

secondary antibodies at room temperature for 2 h, the membranes were washed again. ECL reagent was applied for chemiluminescent detection. Finally, the grayscale values of protein bands were analyzed.

Determination of SOD Enzyme Activity in Colon and Kidney Tissues Using the WST-8 Method

A 0.1 g tissue sample was homogenized with 1 mL of extraction buffer, followed by centrifugation at12000rpm for 10 min. The supernatant was collected as the test sample. Subsequently, reagents and samples were added strictly in accordance with the kit instructions, mixed thoroughly, and incubated in the dark at room temperature for 30 min. Absorbance values of each tube were measured at 450 nm using a microplate reader. SOD enzyme activity was calculated based on the absorbance readings.

Fluorescence-Based Quantification of ROS Intensity in Colon and Kidney Tissues

A 0.1 g tissue sample was homogenized with 1 mL of extraction buffer, followed by centrifugation at 12,000 rpm for 10 min. The supernatant was collected as the test sample. Subsequently, reagents and samples were added strictly in accordance with the kit instructions, mixed thoroughly, and incubated in the dark at room temperature for 30 min. Fluorescence intensity was measured using a microplate reader at an excitation wavelength of 485 nm and an emission wavelength of 535 nm. ROS intensity was calculated based on the fluorescence readings.

High-Throughput Sequencing of 16S rRNA Genes from Colon Contents

Colon content samples were first subjected to preprocessing, followed by total DNA extraction. DNA concentration was quantified using a NanoDrop spectrophotometer (Thermo Scientific, USA), and DNA integrity was assessed via agarose gel electrophoresis. Standard bacterial 16S rRNA V3V4 region primers were selected for PCR amplification, including forward primer 338F (5'-ACTCCTACGGGAGGCAGCA-3') and reverse primer 806R (5'-GGACTACHVGGGTWTCTAAT-3'). The PCR-amplified products were purified and quantified using the Quant-iT PicoGreen dsDNA Assay Kit on a Microplate Reader (BioTek, FLx800). Sequencing libraries were prepared with the Illumina TruSeq Nano DNA LT Library Prep Kit. Qualified libraries underwent paired-end sequencing (2×250 bp) on an Illumina NovaSeq platform using the NovaSeq 6000 SP Reagent Kit (500 cycles). Sequencing was performed by Shanghai Personal Biotechnology Co., LTD (Shanghai, China).

Bioinformatics Analysis

(1) Sequence Processing and Taxonomic Annotation: Raw sequencing data were processed using the QIIME2 DADA2 pipeline to denoise sequences and generate amplicon sequence variants (ASVs). Taxonomic classification was performed by aligning ASV representative sequences against reference sequences in the Greengenes database. For each sample in the ASV abundance matrix, random subsampling of total sequence counts was conducted at varying depths. Using the subsampled sequence counts and corresponding ASV numbers at each depth, rarefaction curves, sequence length distributions, and Venn diagrams were constructed based on ASV abundance data.[29]

(2) Alpha Diversity Analysis: The Shannon index, Simpson index, Chao1 index, and Pielou's evenness index were calculated for each sample group to evaluate variations in gut microbiota richness, diversity, and evenness across groups.

(3) Beta Diversity Analysis: Microbial community structural variations among samples were assessed using the Bray-Curtis dissimilarity algorithm, with visualizations performed through Principal Coordinate Analysis (PCoA) and Non-Metric Multidimensional Scaling (NMDS).

(4) Characteristic Microbiota Analysis: Differential analysis of microbial taxa across all classification levels in inter-group samples was performed using the LDA Effect Size (LEfSe) algorithm, with the LDA threshold set to 2. Random forest analysis was conducted using ASV information.

(5) Correlation Analysis: Spearman's rank correlation coefficients were calculated to evaluate associations between identified microbial genera and SCFAs concentrations in colonic contents, as well as between microbial genera and SOD/

ROS levels in tissues. Redundancy analysis (RDA) was performed to assess relationships between diarrheal clinical signs and tissue SOD/ROS concentrations.

(6) Metabolic Pathway Prediction: Metabolic pathway prediction of the gut microbiota was conducted using the PICRUSt2 analysis pipeline with KEGG database annotations, followed by PCoA of functional units.

Determination of SCFAs Concentrations in Colonic Contents by GC-MS

Quantitative analysis of acetic acid, propionic acid, isobutyric acid, butyric acid, isovaleric acid, and valeric acid concentrations in colonic contents was performed using GC-MS. The analytical services for GC-MS quantification were contracted to Qingdao Yixin Testing Technology Service Co., Ltd. GC-MS conditions and analytical protocols were conducted as previously described.[30]

Statistical Analysis

Statistical analysis and graphing were performed using GraphPad Prism 8.0 software. Data obtained from each group are presented as mean ± standard deviation (mean ± SD). When the data conformed to a normal distribution, an independent samples *t*-test was applied; when the data did not conform to a normal distribution, the Mann–Whitney test was used. A statistically significant difference was indicated when $P < 0.05$, and a highly statistically significant difference was indicated when $P < 0.01$.

Results

General Characteristics of Mice in Each Group

As shown in Figure 1A–C, mice in the CC group exhibited dry bedding, well - formed feces with moderate texture that did not easily adhere to the bedding, and clean perianal regions. In contrast, mice in the CM group displayed damp bedding, loose and unformed feces that easily adhered to the bedding, and perianal regions with fecal attachment and poor cleanliness. Compared with the CC group, mice in the CM group showed a significant decrease in rectal temperature ($P < 0.01$) (Figure 1D) and a significant increase in fecal moisture content ($P < 0.01$) (Figure 1E). These findings indicate alterations in rectal temperature and fecal moisture content in mice with the diarrhea model, characterized by decreased body temperature and increased fecal moisture content.

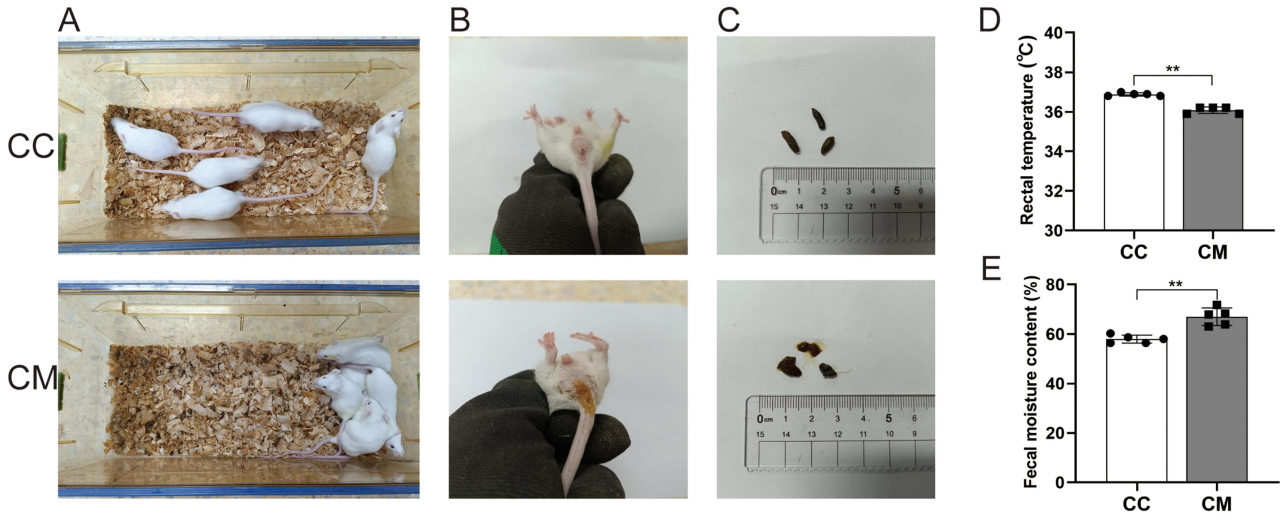

Figure 1 General conditions of mice in each group. (**A**) Mental status and bedding conditions of mice in each group; (**B**) Perianal cleanliness of mice in each group; (**C**) Fecal characteristics of mice in each group; (**D**) Rectal temperatures of mice in each group; (**E**) Fecal moisture contents of mice in each group. n=5, ** $P < 0.01$. CC: normal group; CM: diarrhea model group.

https://doi.org/10.2147/JIR.S588857

Alterations in Histological Morphology of Colon and Kidney Tissues in Mice Among Different Groups

As shown in Figure 2A, the tissue architecture of each layer in the colon of mice from the CC group exhibited no significant abnormalities, with crypts arranged in a parallel and orderly manner and no obvious abnormal inflammatory infiltration observed. As shown in Figure 2B, the crypt architectures within the colonic tissues of mice belonging to the CM group demonstrated signs of atrophy and branching, which was accompanied by abnormal inflammatory infiltration in the tissues and an increased number of inflammatory cells within the field of view.

As depicted in Figure 2C, the renal cortex of mice within the CC group presented a well - defined structure. There was neither a marked increase nor a notable decrease in the volume of glomeruli. Moreover, the glomerular capsular spaces were clearly visible, and there was no tubular wall atrophy or lumen dilation, nor was there any obvious inflammatory cell infiltration in the interstitium. In contrast, as shown in Figure 2D, the renal cortex of mice in the CM group exhibited structural damage, with a large number of inflammatory cells present in the glomeruli, unclear glomerular capsular spaces, and irregular tubular lumen structures.

Changes in the Molecules Related to the SIRT3-SOD2-ROS Pathway in Colon and Kidney Tissues of Mice Across Different Groups

Changes in the Relative Expression Levels of SIRT3 and SOD2 Proteins in Colon and Kidney Tissues of Mice Across Different Groups

Compared with the CC group, the relative expression level of SIRT3 protein in the colon tissue of mice in the CM group was significantly decreased ($P < 0.01$) (Figure 3A and B), and the relative expression level of SOD2 protein in the colon tissue of mice in the CM group was also significantly reduced ($P < 0.01$) (Figure 3A and C). Similarly, when compared with the CC group, the relative expression level of SIRT3 protein in the kidney tissue of mice in the CM group showed a significant decrease ($P < 0.01$) (Figure 3D and E), and the relative expression level of SOD2 protein in the kidney tissue of mice in the CM group was significantly lowered as well ($P < 0.01$) (Figure 3D and F).

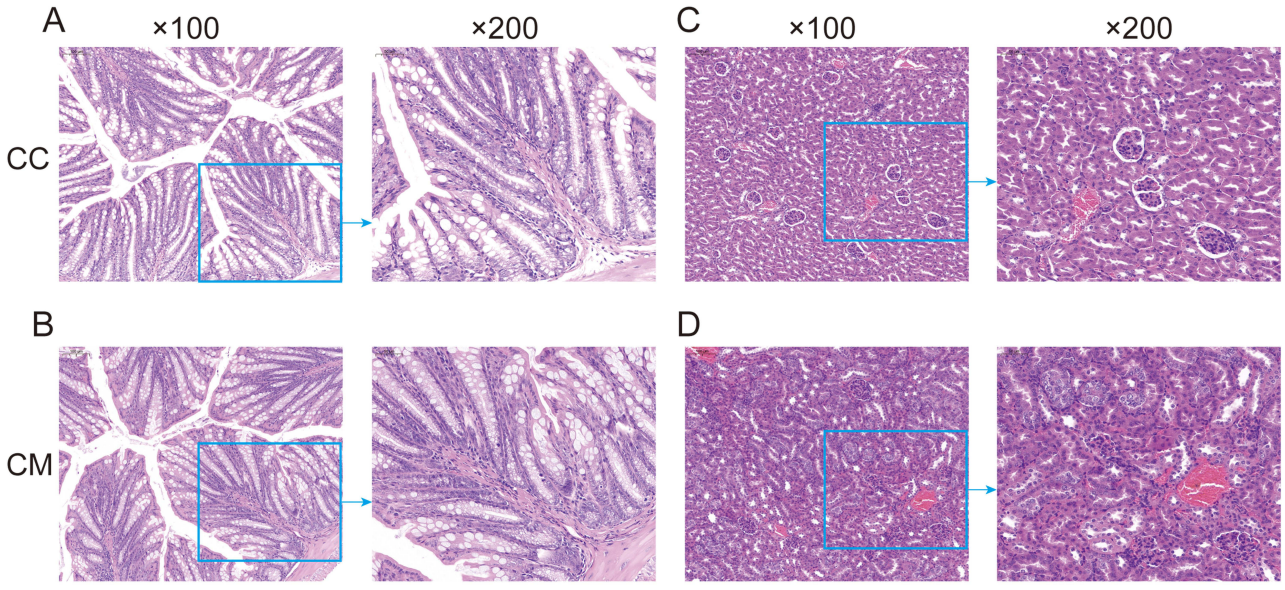

Figure 2 Alterations in histological morphology of colon and kidney tissues in mice among different groups. (**A**) HE staining of colon tissue in mice from the CC group (×100, ×200); (**B**) HE staining of colon tissue in mice from the CM group (×100, ×200); (**C**) HE staining of kidney tissue in mice from the CC group (×100, ×200); (**D**) HE staining of kidney tissue in mice from the CM group (×100, ×200). CC: normal group; CM: diarrhea model group.

https://doi.org/10.2147/JIR.S588857

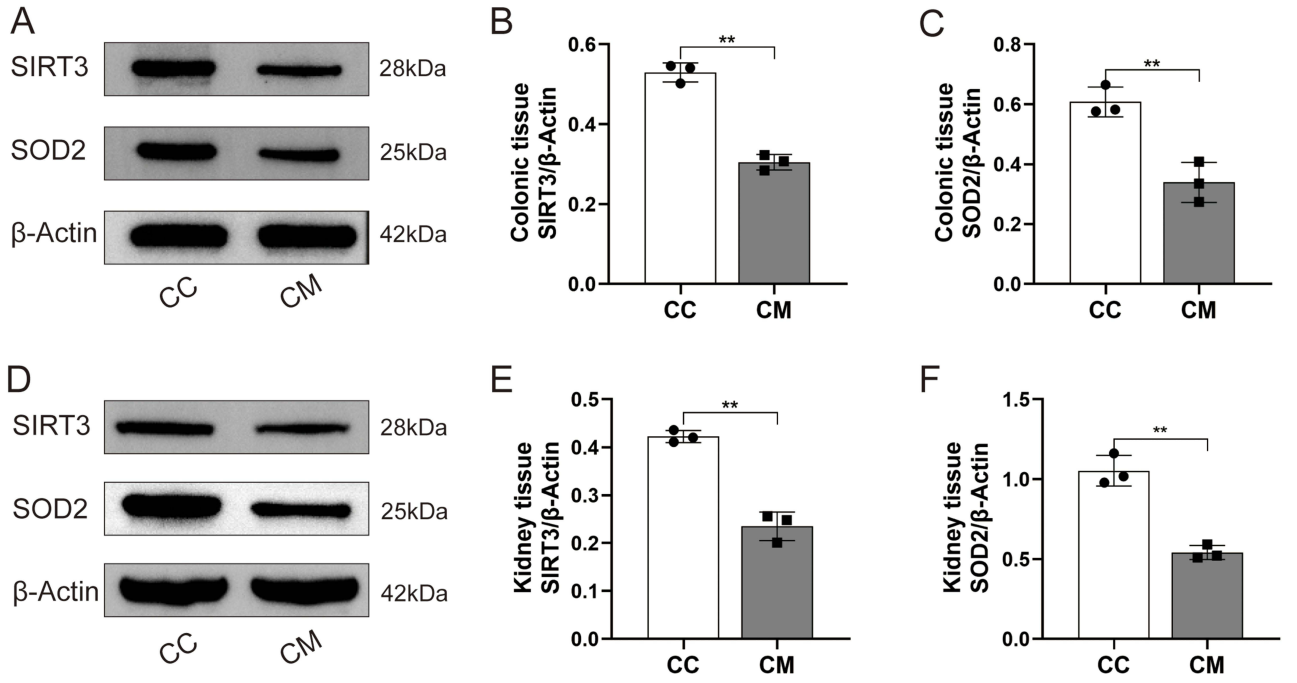

Figure 3 Changes in the relative expression levels of SIRT3 and SOD2 proteins in colon and kidney tissues of mice across different groups. (**A**) Western blot images of SIRT3 and SOD2 proteins in colon tissue; (**B**) Statistical analysis of the relative expression level of SIRT3 protein in colon tissue; (**C**) Statistical analysis of the relative expression level of SOD2 protein in colon tissue; (**D**) Western blot images of SIRT3 and SOD2 proteins in kidney tissue; (**E**) Statistical analysis of the relative expression level of SIRT3 protein in kidney tissue; (**F**) Statistical analysis of the relative expression level of SOD2 protein in kidney tissue. n = 3, ** $P < 0.01$. CC: normal group; CM: diarrhea model group.

Changes in SOD Enzyme Activity and ROS Intensity in Colon and Kidney Tissues of Mice Across Different Groups

Compared with the CC group, the SOD enzyme activity in the colon tissue of mice in the CM group was significantly decreased ($P < 0.05$) (Figure 4A), and the SOD enzyme activity in the kidney tissue of mice in the CM group was also significantly reduced ($P < 0.01$) (Figure 4B). In comparison with the CC group, the ROS intensity in the colon tissue of mice in the CM group was significantly elevated ($P < 0.01$) (Figure 4C), and the ROS intensity in the kidney tissue of mice in the CM group was likewise significantly increased ($P < 0.01$) (Figure 4D).

Analysis of Microbial Community Structure and Function in Colonic Contents

Quality Assessment of Gut Microbiota Sequencing Data and Sample ASV Numbers

As shown in Figure 5A, the Shannon rarefaction curves gradually flattened with increasing sequencing depth across samples, indicating that the sequencing coverage in this study was sufficiently comprehensive to reflect the species composition and estimate community richness of the microbial communities. Figure 5B illustrates the ASV counts across sample groups: the CC group contained 5269 ASVs, of which 4332 were unique; the CM group contained 4693 ASVs, with 3756 being unique. A total of 937 ASVs were shared between the two groups.

Compared with the CC group, the CM group exhibited a decreasing trend in the Shannon index, Simpson index, Chao1 index, and Pielou's evenness index; however, these differences were not statistically significant ($P > 0.05$) (Figure 5C–F). This indicates that, relative to normal mice, the model mice demonstrated reduced species richness, evenness, and diversity in the gut microbiota of the colon. In the NMDS analysis (Figure 5G), NMDS analysis showed a moderate separation tendency between the CC and CM groups (stress=0.239), suggesting potential differences in microbial community structure. In the PCoA analysis (Figure 5H), the PCo1 explained 27.7% of the total variance, and the PCo2 explained 16.8% of the total variance. The projected distances between samples from the CC and CM groups were relatively large, with no complete overlap observed. These findings suggest that the microbial community structure in the colonic contents of model mice differs significantly from that of normal mice.

https://doi.org/10.2147/JIR.S588857

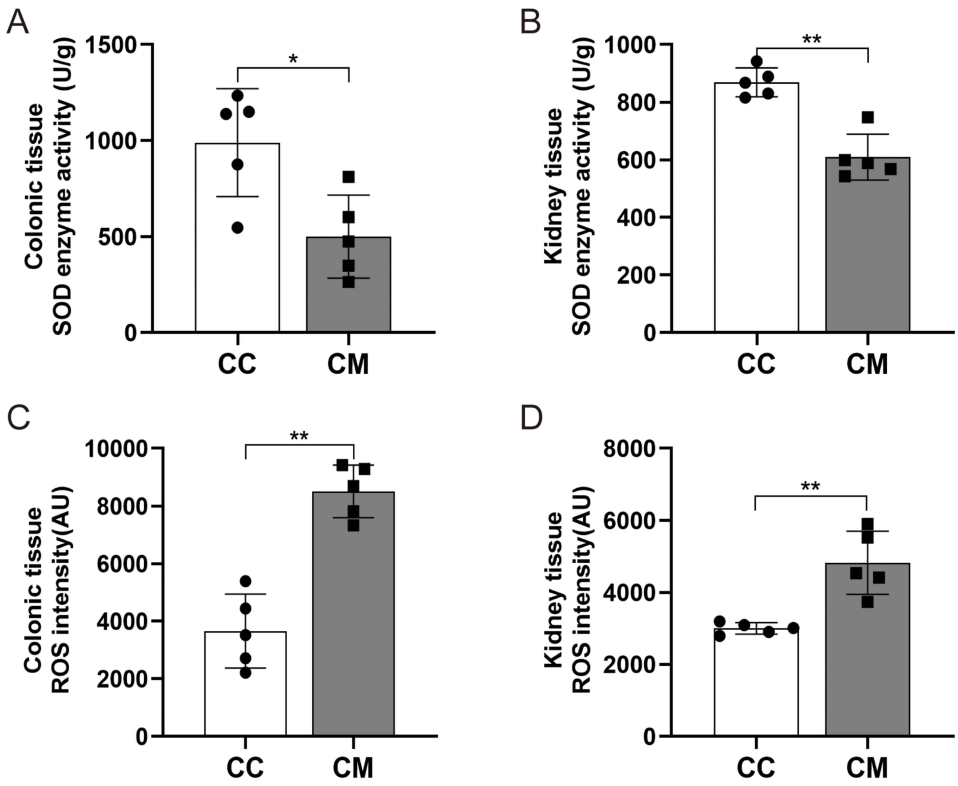

Figure 4 Changes in SOD enzyme activity and ROS intensity in colon and kidney tissues of mice across different groups. (**A**) SOD enzyme activity in colon tissue; (**B**) SOD enzyme activity in kidney tissue; (**C**) ROS intensity in colon tissue; (**D**) ROS intensity in kidney tissue. n = 5, * $P < 0.05$, ** $P < 0.01$. CC: normal group; CM: diarrhea model group.

Changes in Species Composition of the Gut Microbiota

As shown in Figure 6A, differences in the number of taxonomic units at all classification levels were observed between the CC and CM groups, with the CC group exhibiting a greater richness of gut microbiota taxonomic units compared to the CM group. Figure 6B illustrates the top 10 most abundant phyla in the gut microbiota; the three most dominant phyla were Firmicutes (50.54% in CC, 63.56% in CM), Bacteroidetes (41.46% in CC, 29.56% in CM), and Proteobacteria (4.35% in CC, 4.46% in CM). Figure 6C displays the top 15 most abundant genera in the gut microbiota; the top five genera in the CC group were *Lactobacillus* (23.72%), *[Prevotella]* (4.64%), *Oscillospira* (2.92%), *Odoribacter* (2.45%), and *Candidatus Arthromitus* (1.63%), whereas those in the CM group were *Lactobacillus* (33.34%), *[Prevotella]* (5.92%), *Bacteroides* (3.35%), *Oscillospira* (2.79%), and *Ruminococcaceae_Ruminococcus* (1.93%).

Further statistical analysis of the relative abundances of Firmicutes, Bacteroidota, and the Firmicutes/Bacteroidota ratio revealed that compared to the CC group, the CM group exhibited an increasing trend in Firmicutes relative abundance, a decreasing trend in Bacteroidota relative abundance, and an elevated Firmicutes/Bacteroidota ratio, though no significant differences were observed for these parameters (Figure 6D–F). Statistical analysis of equal abundance among the top 10 phyla and top 15 genera by relative abundance identified significant differences in *Cyanobacteria* and *Streptococcus* between the two groups. Compared to the CC group, the CM group demonstrated significantly reduced relative abundance of *Cyanobacteria* ($P < 0.05$) (Figure 6G) and significantly increased relative abundance of *Streptococcus* ($P < 0.01$) (Figure 6H).

Differential Analysis of Gut Microbiota Composition

As shown in Figure 7A and B, LEfSe analysis was performed with an LDA threshold set at 2, identifying 10 robust differentially abundant taxa. *Cyanobacteria, 4C0d_2, YS2*, and *Peptococcaceae* were identified as significantly enriched taxa in the CC group, while *Bifidobacteriales, Bifidobacteriaceae, Streptococcaceae, Bifidobacterium, Streptococcus*, and *Erysipelotrichaceae_Clostridium* were significantly enriched in the CM group. As shown in Figure 7C, further random

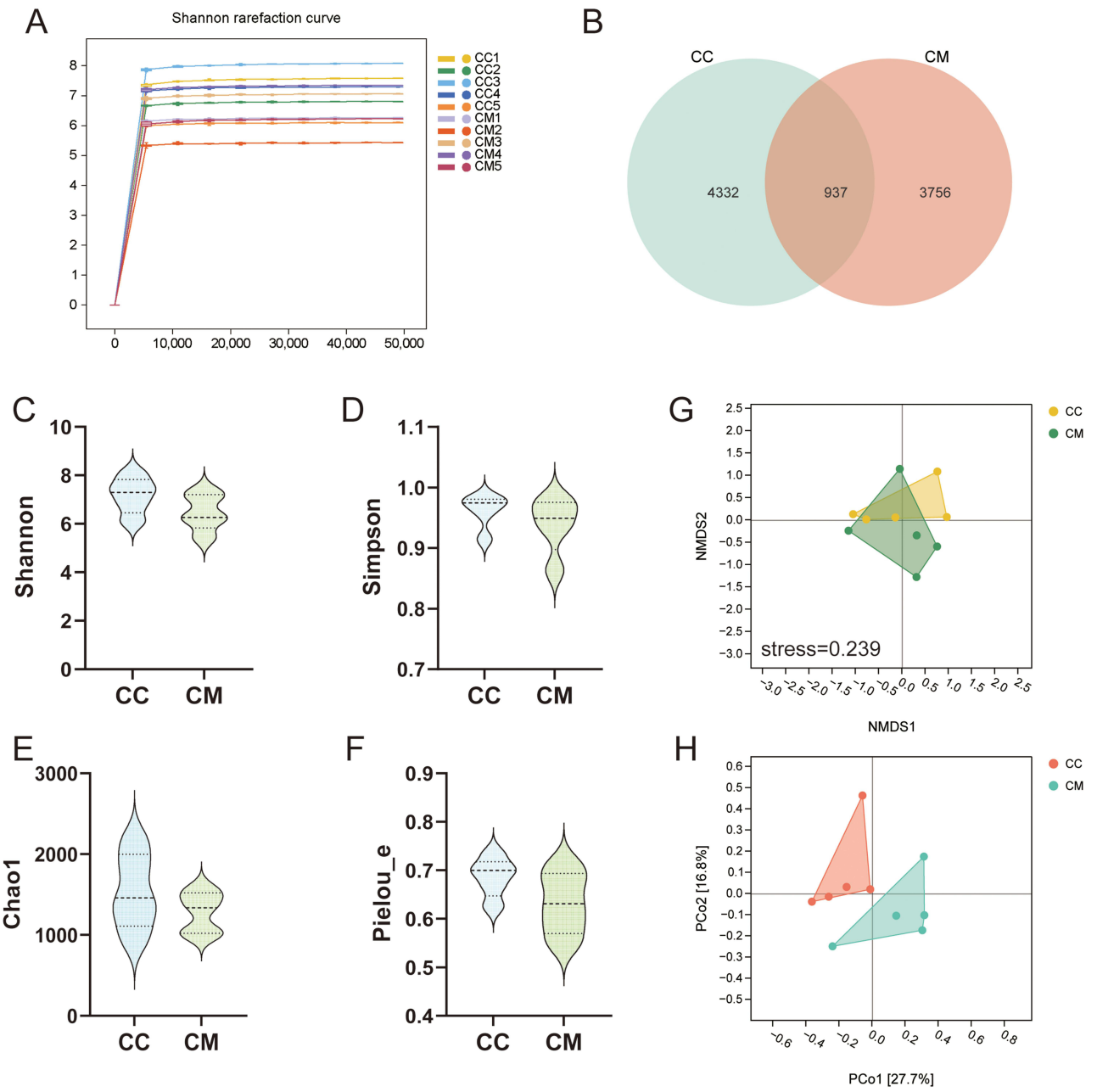

Figure 5 Quality assessment and Alpha/Beta diversity analysis of gut microbiota sequencing data. (**A**) Shannon rarefaction curve; (**B**) Venn diagram; (**C**) Shannon index; (**D**) Simpson index; (**E**) Chao1 index; (**F**) Pielou's evenness index; (**G**) NMDS analysis; (**H**) PCoA analysis. n = 5; CC: normal group; CM: diarrhea model group.

forest analysis identified the top 10 genera ranked by importance, listed in descending order: *Streptococcus, Butyricicoccus, Bifidobacterium, Sutterella, Mucispirillum, Candidatus Arthromitus, Akkermansia, Helicobacter, Alistipes*, and *Rummeliibacillus*.

Predictive Analysis of Gut Microbiota Metabolic Functions

Based on the KEGG metabolic pathway database, PICRUSt2 analysis was employed to predict metabolic functions from the 16S rRNA sequencing data obtained in this experiment. As shown in Figure 8A, the first-level metabolic pathways of colonic content microbiota were classified into six categories, with 33 second-level pathways identified. The first-level pathways comprised: Cellular Processes, Environmental Information Processing, Genetic Information Processing, Human Diseases, Metabolism, and Organismal Systems, among which the Metabolism pathway exhibited the highest

https://doi.org/10.2147/JIR.S588857

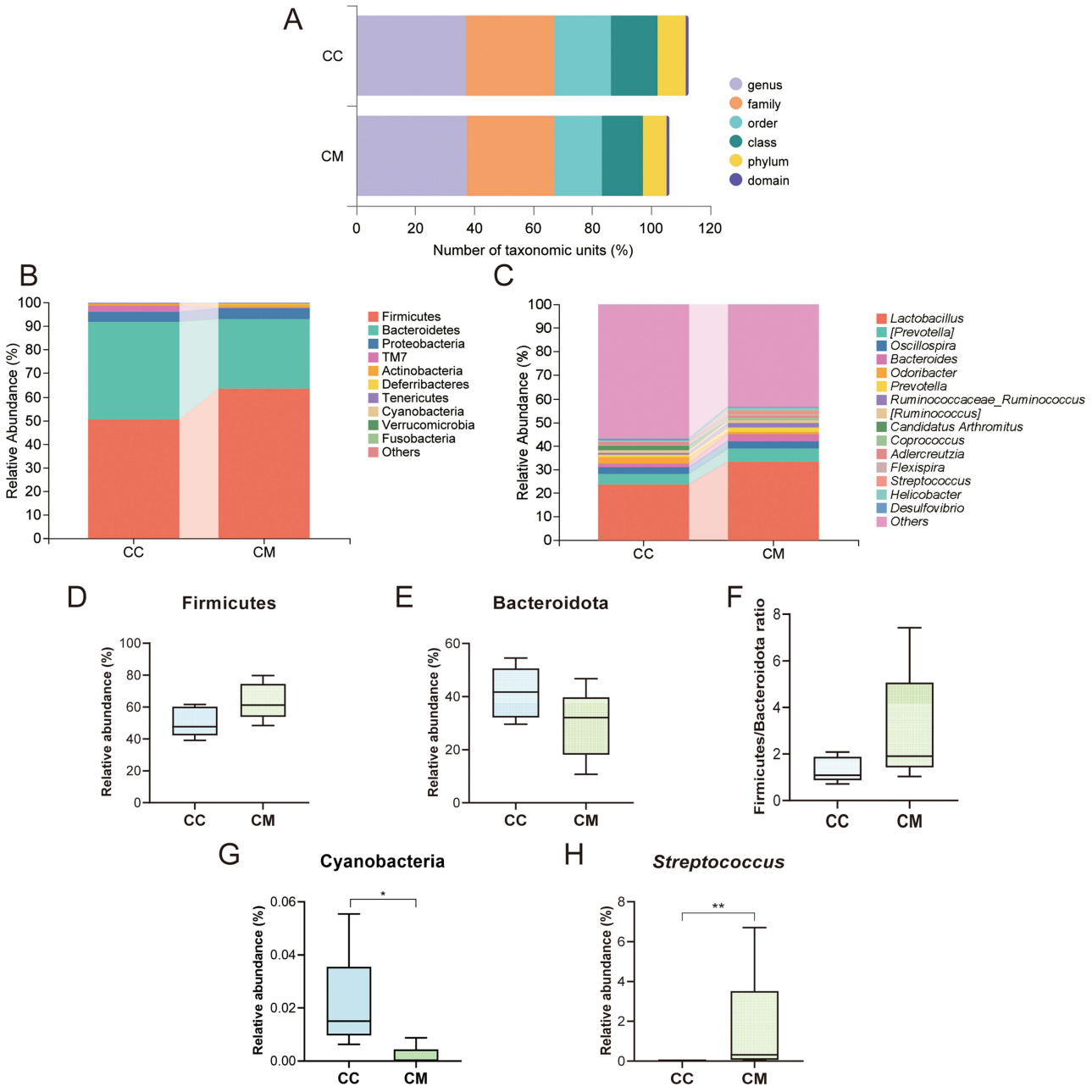

Figure 6 Changes in species composition of the gut microbiota. (**A**) Number of taxonomic units at each classification level; (**B**) Top 10 phyla ranked by relative abundance; (**C**) Top 15 genera ranked by relative abundance; (**D**) Statistical analysis of Firmicutes relative abundance; (**E**) Statistical analysis of Bacteroidota relative abundance; (**F**) Statistical analysis of Firmicutes/Bacteroidota ratio; (**G**) Statistical analysis of Cyanobacteria relative abundance; (**H**) Statistical analysis of Streptococcus relative abundance. n = 5, * $P < 0.05$, ** $P < 0.01$. CC: normal group; CM: diarrhea model group.

relative abundance. Within the Metabolism category, 11 second-level pathways were identified: Amino acid metabolism, Biosynthesis of other secondary metabolites, Carbohydrate metabolism, Energy metabolism, Glycan biosynthesis and metabolism, Lipid metabolism, Metabolism of cofactors and vitamins, Metabolism of other amino acids, Metabolism of terpenoids and polyketides, Nucleotide metabolism, and Xenobiotics biodegradation and metabolism. As shown in Figure 8B, after conducting PCoA analysis on functional units, it was found that the projections of samples from the CC group and the CM group on the coordinate axes exhibited a relatively separated state, yet there was a certain degree of overlap. Specifically, PCoA1 accounted for 58.9% of the total variation proportion, while PCoA2 explained the remaining 21.1% of the variance proportion. The sum of the explanatory proportions of PCoA1 and PCoA2 was 80%,

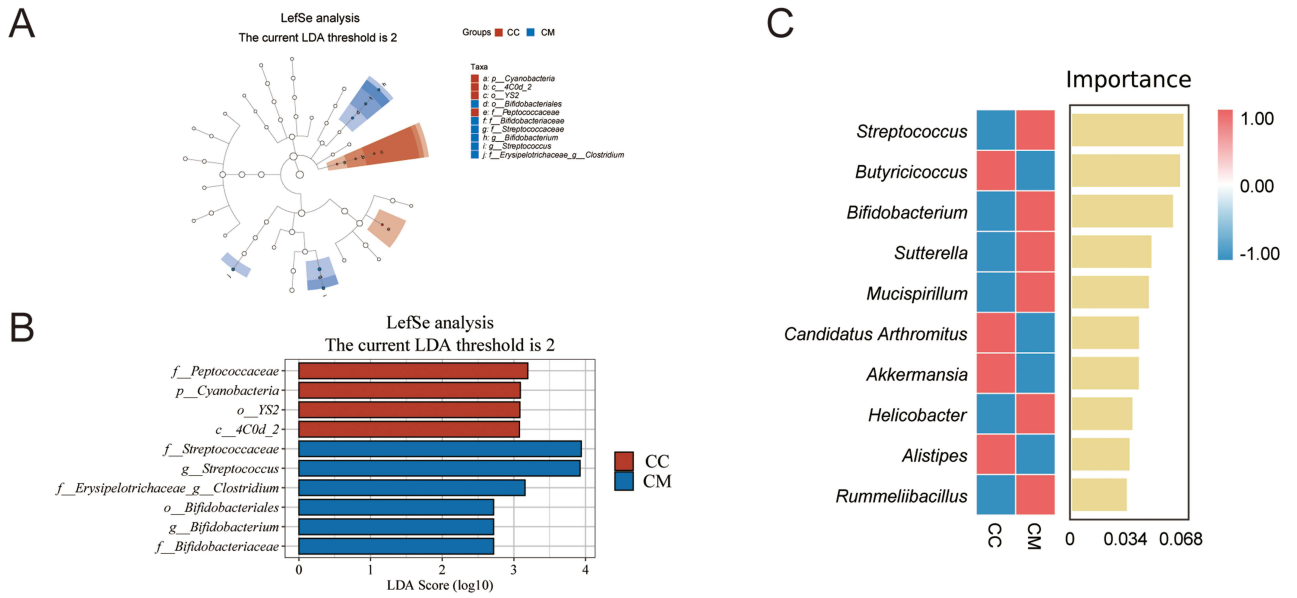

Figure 7 Differential analysis of gut microbiota composition. (**A**) Cladogram generated by LEfSe analysis; (**B**) Bar plot from LEfSe analysis; (**C**) Top 10 genera ranked by importance from random forest analysis. n = 5; CC: normal group; CM: diarrhea model group.

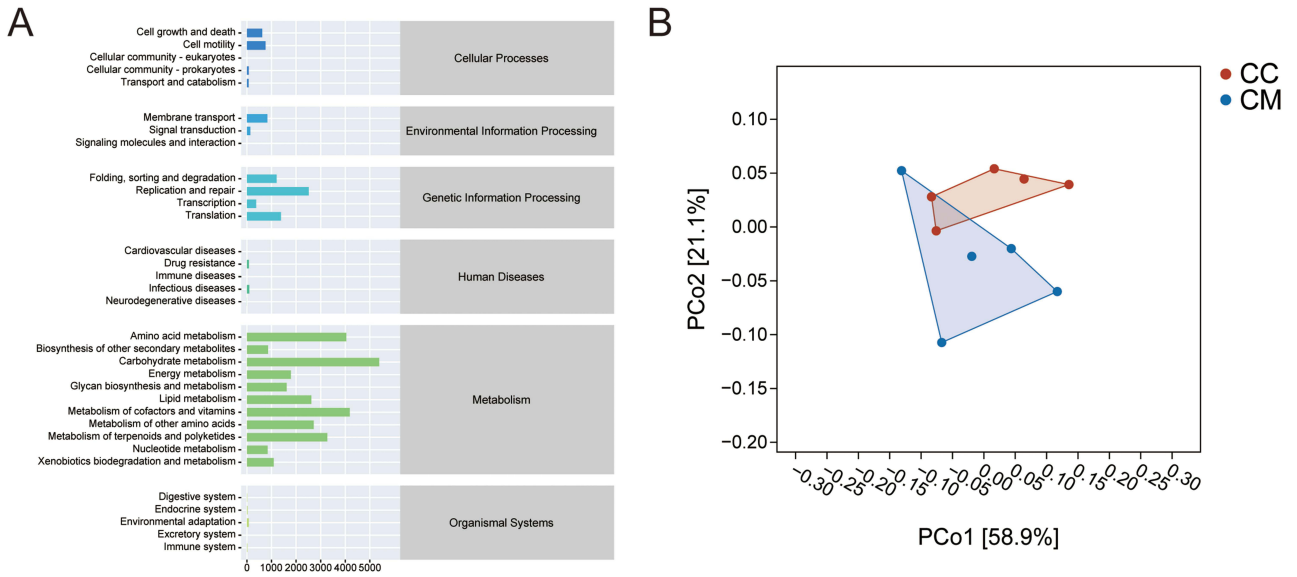

Figure 8 Predictive analysis of gut microbiota metabolic functions. (**A**) Predicted Level 1 and Level 2 metabolic pathways based on KEGG; (**B**) Functional unit PCoA analysis. CC: normal group; CM: diarrhea model group.

indicating that these two principal coordinate axes could effectively summarize the main structure of the data, and further demonstrating that the distribution pattern of the samples had a relatively high level of credibility.

Changes in SCFAs Levels in Colonic Contents Across Mouse Groups

As shown in Figure 9, compared with the CC group, the CM group exhibited significantly reduced levels of propionic acid and isobutyric acid in colonic contents ($P < 0.05$). Acetic acid, butyric acid, isovaleric acid, and valeric acid levels demonstrated a downward trend, although there was no statistically significant difference. These findings suggest abnormal levels of SCFAs in the colonic contents of model mice.

https://doi.org/10.2147/JIR.S588857

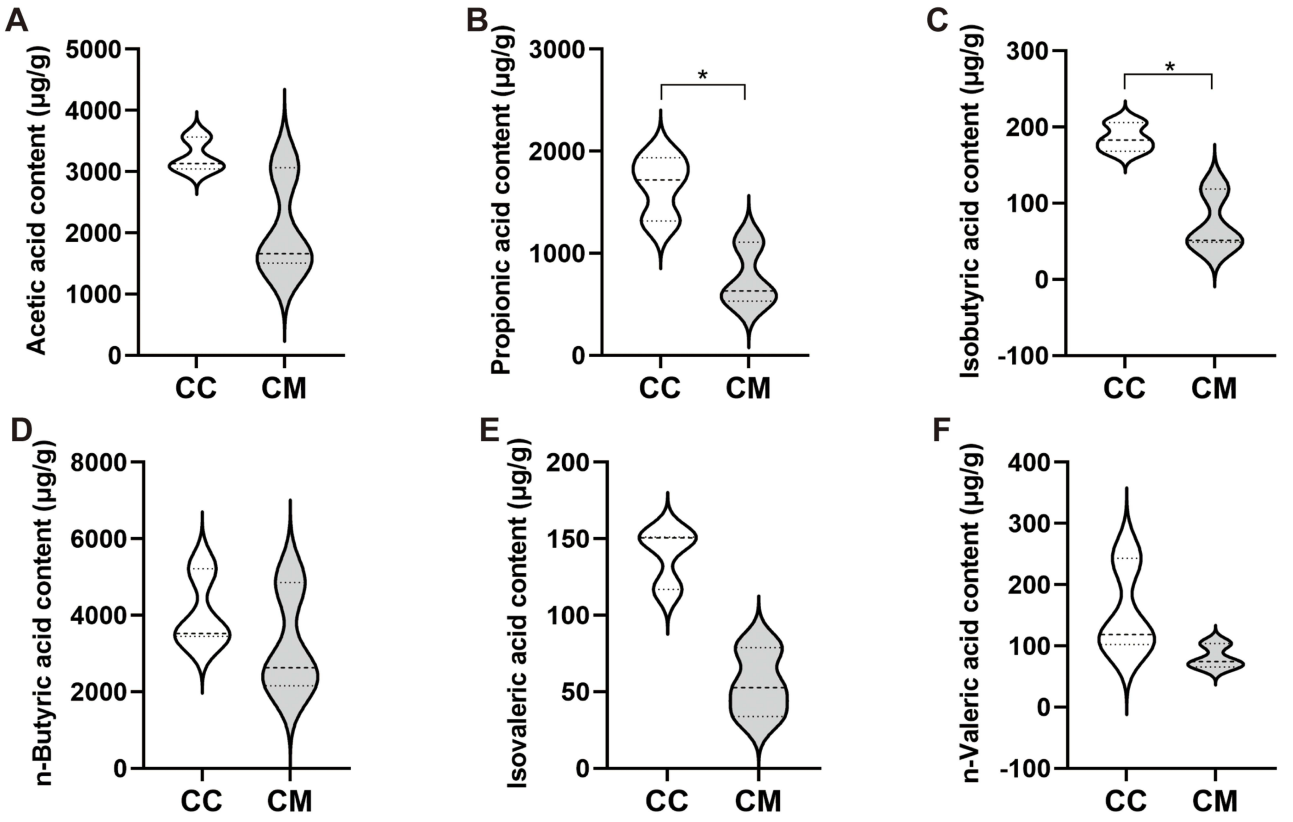

Figure 9 Changes in SCFAs levels in colonic contents. (**A**) Acetic acid content; (**B**) Propionic acid content; (**C**) Isobutyric acid content; (**D**) Butyric acid content; (**E**) Isovaleric acid content; (**F**) Valeric acid content. n = 3, * $P < 0.05$. CC: normal group; CM: diarrhea model group.

Correlation Analysis

Correlation Analysis Between Characteristic Bacterial Genera in Colonic Contents and SCFAs

Spearman correlation analysis was performed between the top 10 characteristic bacterial genera identified by random forest analysis and the levels of acetic acid, propionic acid, isobutyric acid, butyric acid, isovaleric acid, and valeric acid in colonic contents. As shown in Figure 10A, the characteristic genera *Alistipes* and *Candidatus Arthromitus* exhibited positive correlations with SCFAs. In contrast, *Flexispira, Rummeliibacillus, Streptococcus, Mucispirillum*, and *Sutterella* demonstrated negative correlations with SCFAs. *Butyricicoccus* displayed a negative correlation with acetic acid but positive correlations with other SCFAs. *Akkermansia* showed a positive correlation with acetic acid and negative correlations with other SCFAs. *Bifidobacterium* demonstrated a positive correlation with butyric acid and negative correlations with other SCFAs.

Correlation Between Characteristic Bacterial Genera in Colonic Contents and SOD/ROS Levels in Colonic and Kidney Tissues

As shown in Figure 10B, *Alistipes, Candidatus Arthromitus, Butyricicoccus*, and *Akkermansia* exhibited a positive correlation with SOD enzyme activity in colonic and kidney tissues; *Bifidobacterium, Mucispirillum, Rummeliibacillus, Streptococcus, Sutterella*, and *Flexispira* showed a negative correlation with SOD enzyme activity in colonic and kidney tissues. *Bifidobacterium, Mucispirillum, Rummeliibacillus, Streptococcus, Sutterella*, and *Flexispira* were positively correlated with ROS intensity in colonic and kidney tissues. *Alistipes, Candidatus Arthromitus, Butyricicoccus*, and *Akkermansia* were negatively correlated with ROS intensity in colonic and kidney tissues.

Correlation Analysis Between Diarrhea Sign Indicators and SOD/ROS Levels in Colonic and Kidney Tissues

As shown in the RDA analysis of Figure 10C, rectal temperature exhibited a positive correlation with SOD levels in colonic and kidney tissues, whereas fecal moisture content demonstrated a negative correlation with SOD levels in these tissues. As

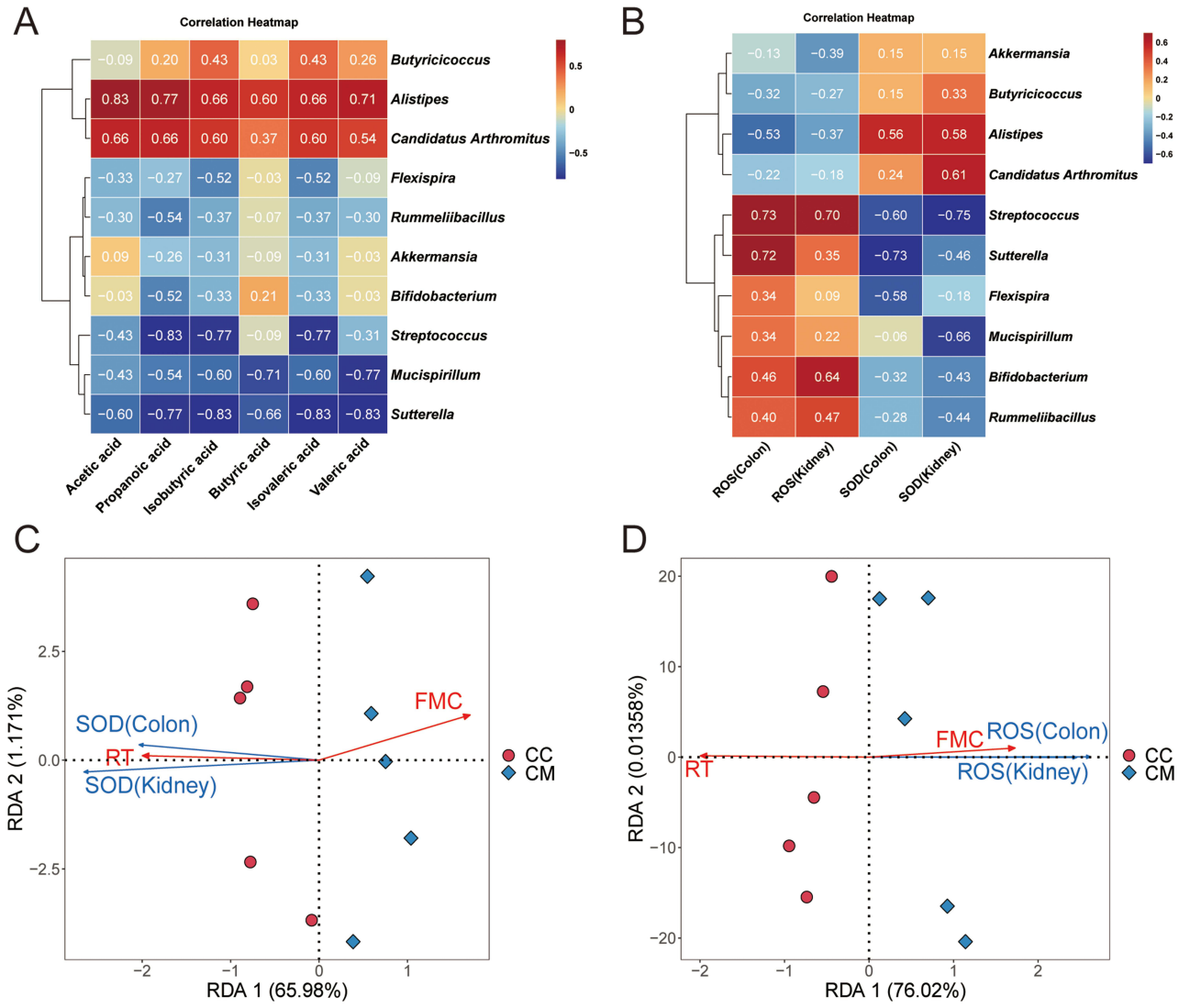

Figure 10 (**A**) Heatmap of correlation coefficients between characteristic microbial genera in colonic contents and SCFAs; (**B**) Heatmap of correlation coefficients between characteristic bacterial genera and levels of SOD and ROS; (**C**) RDA analysis of diarrhea sign indicators versus SOD levels in tissues; (**D**) RDA analysis of diarrhea sign indicators versus ROS levels in tissues. CC: normal group; CM: diarrhea model group.
Abbreviations: RT, rectal temperature; FMC, fecal moisture content.

depicted in the RDA analysis of Figure 10D fecal moisture content displayed a positive correlation with ROS levels in colonic and kidney tissues, while rectal temperature showed a negative correlation with ROS levels in these tissues.

Discussion

The Molecules Related to the SIRT3-SOD2-ROS Pathway are a Critical Mediator of Gut-Kidney Interaction Injury in Renal-Associated Diarrhea

Oxidative stress and inflammatory responses have been confirmed to play pivotal roles in the complex pathological mechanisms of intestinal-related diseases.[31–33] The intestinal inflammatory microenvironment contains excessive reactive ROS. Elevated ROS levels coupled with reduced antioxidant capacity induce oxidative stress imbalance, which causes oxidation of proteins and lipids as well as DNA damage, ultimately leading to intestinal epithelial cell injury.[34] Overabundant ROS promote tissue inflammation and activate immune responses through NLRP3 inflammasome signaling.[35,36] In this study, we observed significantly increased ROS intensity in colonic and kidney tissues of model mice, indicating systemic imbalance between oxidation and antioxidant functions that results in oxidative stress injury.

https://doi.org/10.2147/JIR.S588857

Antioxidant defense mechanisms depend on key enzymes including SOD, catalase (CAT), and glutathione peroxidase (GPX). These enzymes neutralize ROS to counteract oxidative damage and maintain cellular redox homeostasis.[37] SOD primarily executes antioxidant defense by converting superoxide radicals into molecular oxygen and hydrogen peroxide, thereby eliminating intracellular ROS and establishing a negative feedback regulatory mechanism.[38,39] The deacetylase activity of SIRT3 effectively enhances SOD2 enzymatic activity.[40]

We measured the relative protein expression levels of SIRT3 and SOD2, as well as SOD enzymatic activity, in colonic and kidney tissues of model mice. Our findings revealed significant reductions in all parameters, indicating that decreased SIRT3 and SOD2 protein levels coupled with diminished SOD activity in these tissues impaired the effective clearance of excessive ROS. This resulted in exacerbated oxidative stress injury and structural damage to both colonic and kidney tissues. Therefore, the molecules related to the SIRT3 - SOD2 - ROS pathway are closely associated with the pathogenesis of renal-associated diarrhea, representing a key mechanism underlying gut-kidney interaction injury in this condition.

Species Alterations of Gut Microbiota in the Colon, Altered Levels of SCFAs, and Gut-Kidney Oxidative Stress are Closely Associated with the Onset and Progression of Renal-Associated Diarrhea

Under normal physiological conditions, the gut microbiota structure, microbial functions, metabolic products, and their intricate interactions with the host collectively establish the intestinal microecosystem. This system typically sustains its structural composition, species diversity, and microbial load at relatively stable levels, thereby playing a pivotal role in both maintaining human health and influencing disease progression.[41] The gut microbiota demonstrates close associations with multiple factors involved in biological processes, including sex, age, physiological/pathological states, lifestyle habits, and psychological factors.[42–44] Gut microbiota dysbiosis refers to alterations in the original microbial community and its derived metabolites (eg, SCFAs), leading to a reduction in beneficial bacteria and/or an expansion of pathogenic bacteria.[45,46]

This study revealed that in the colon of mice from the model group, the species richness, evenness, and diversity of the gut microbiota were significantly reduced, with distinct alterations in the microbial community structure of colonic contents compared to normal mice. Concurrently, we observed a marked decrease in the relative abundance of Cyanobacteria ($P < 0.05$) and a significant increase in *Streptococcus* ($P < 0.01$) in the model group. Research on intestinal Cyanobacteria remains in its infancy, though these organisms are known to participate in food digestion and absorption. Notably, fecal samples from patients with gastrointestinal and hepatic diseases exhibit significant differences in Cyanobacteria abundance between healthy controls and disease groups, yet no consistent positive or negative correlations have been identified.[47] Naturally derived Cyanobacteria produce a diverse array of secondary metabolites[48,49] with potent antioxidant, anti-inflammatory, anticancer, and hypolipidemic effects.[50] They scavenge ROS and modulate gene expression involved in antioxidant enzyme synthesis and other stress response proteins, thereby maintaining an appropriate balance between ROS and antioxidant defenses.[51,52]

Both LEfSe and random forest analyses similarly identified *Streptococcus* as significantly enriched in the colonic region of mice from the model group. The genus *Streptococcus* comprises over 100 identified species that constitute part of the human or animal microbiota, including multiple clinically significant pathogens.[53] As a potential specific microbial biomarker, *Streptococcus* has been associated with gastrointestinal disorders, infections, or autoimmune diseases.[54–56] Many Streptococcus species act as opportunistic pathogens capable of inducing infections under conditions of relatively weakened host immune responses.[57] Correlation analyses revealed a significant negative association between Streptococcus abundance and SOD enzyme activity in kidney tissues ($P < 0.05$), along with positive correlations with ROS intensity in both colonic and kidney tissues ($P < 0.05$). Consequently, *Streptococcus*, which was significantly enriched in the colonic microbiota of model group mice, may represent a key bacterium influencing molecules related to the SIRT3-SOD2-ROS pathway, thereby contributing to intestinal and kidney oxidative stress and inflammatory responses associated with renal-associated diarrhea.

SCFAs play a crucial role in maintaining intestinal homeostasis, strengthening intestinal barrier function, and exhibiting anti-inflammatory activity, while serving as the primary energy source for colonic epithelial cells. Notably, varying degrees of reduction or alteration in SCFAs levels have been observed in gastrointestinal diseases including inflammatory bowel disease,[58] ulcerative colitis,[59] and necrotizing enterocolitis.[60] Consistent with previous studies, the colonic contents of model group mice demonstrated a downward trend in the levels of acetic acid, propionic acid, isobutyric acid, n-butyric acid, isovaleric acid, and n-valeric acid, with significant reductions in propionic acid and isobutyric acid contents ($P < 0.05$). In this study, the number of biological replicates used for SCFA measurements was relatively limited. Nevertheless, we still observed trends in SCFA levels between the model and control groups. Future studies with larger sample sizes will be conducted to enhance the robustness of our conclusions. Bacterial genera such as *Streptococcus, Sutterella, Mucispirillum*, etc, exhibit a negative correlation with the levels of SCFAs. Specifically, the correlation coefficient (R) between *Streptococcus* and propanoic acid is −0.83. The correlation coefficient (R) between *Sutterella* and isobutyric acid, isovaleric acid, as well as valeric acid is −0.83.

Propionate exerts a broad range of biological effects, spanning from maintaining intestinal mucosal integrity to regulating innate and adaptive immune responses at both local and systemic levels.[61] Propionate and butyrate, when combined, directly suppress LPS-induced maturation of monocyte-derived dendritic cells in vitro, thereby reducing IL-12 secretion and limiting $CD8^+$ T cell activation.[62] Mechanistically, propionate binds to G protein-coupled receptor 43 (GPR43) on intestinal epithelial surfaces, promoting histone acetylation and increasing expression of the tight junction proteins occludin and ZO-1. These molecular events elevate mucin levels, thereby reinforcing intestinal epithelial barrier integrity and alleviating radiation-induced intestinal injury.[63] Isobutyric acid supplementation significantly enhances total antioxidant capacity (T-AOC) and SOD levels in animal serum while improving intestinal mucosal barrier function.[64] Consequently, alterations in gut microbial composition in the colon, as well as altered levels of SCFAs and molecules related to the SIRT3-SOD2-ROS pathway are interconnected, which leads to an imbalance in gut-kidney oxidative stress that may influence the onset and progression of diarrhea.

Limitations

There are certain limitations in this study that warrant explanation. Firstly, the sample sizes were relatively small, particularly for sequencing and some molecular assays, which may have constrained the statistical power and generalizability of our findings. Secondly, although the Adenine+*Folium sennae* induced model is widely employed, it may not fully represent the complexity and heterogeneity of specific types of diarrhea in humans. Thirdly, the correlation analyses conducted in this study were unable to establish causal relationships among the gut microbiota, short - chain fatty acids, and molecules associated with the SIRT3 - SOD2 - ROS pathway. Finally, only male mice were used in this study to minimize variability. However, given the sexual dimorphism of the gut microbiota, the absence of female mice may limit the general applicability of the research results.

To validate and expand upon these findings, studies with larger sample sizes that incorporate female mice should be carried out to enhance the robustness of our conclusions. Intervention experiments, such as SCFA supplementation and the administration of agonists/inhibitors, should be conducted to verify the underlying causal relationships.

Conclusion

In summary, the microbial community structure in the colonic contents of diarrhea model mice underwent alterations, with a reduction in microbial richness, evenness, and species diversity. Bacterial genera such as *Streptococcus* were enriched in the colon. The levels of propionic acid and isobutyric acid significantly decreased, and a negative correlation was observed between *Streptococcus* and propionic acid. The relative expression levels of SIRT3 and SOD2 proteins, as well as SOD enzyme activity, significantly decreased in both colonic and kidney tissues, while ROS intensity significantly increased. Correlations were found between *Streptococcus* and SOD enzyme activity, as well as ROS intensity in the tissues. Therefore, alterations in gut microbial composition in the colon, as well as altered levels of SCFAs and molecules related to the SIRT3-SOD2-ROS pathway, have a potential link and serve as important factors contributing to the progression of diarrhea. However, in the future, intervention experiments such as SCFA supplementation and agonist/inhibitor administration will be needed to verify the causal relationship underlying it.

Data Sharing Statement

The gut microbiota sequencing data that support the findings of this study are openly available in the NCBI database at https://www.ncbi.nlm.nih.gov/, reference number PRJNA1353860.

Acknowledgments

Thanks to the National Natural Science Foundation of China (82575001) for supporting this research. Thanks to all the authors for their dedication.

Author Contributions

Junxi Shen: Writing–original draft preparation, software, data curation, visualization.

Leyao Fang: Writing–review and editing, Validation.

Xinxin Peng: Writing - review and editing, Validation.

Miao Jiang: Writing - review and editing, Validation.

Xuejiao Xie: Writing - review and editing, Validation, Supervision.

Zhoujin Tan: Writing - review and editing, Conceptualization, Supervision, Project administration, funding acquisition.

All authors gave final approval of the version to be published; have agreed on the journal to which the article has been submitted; and agree to be accountable for all aspects of the work.

Funding

This work was supported by the National Natural Science Foundation of China (82575001).

Disclosure

The authors have no competing interests to declare that are relevant to the content of this article.

References

1. Zhang M, Qin Z, Huang C, et al. The gut microbiota modulates airway inflammation in allergic asthma through the gut-lung axis related immune modulation: a review. *Biomol Biomed*. 2025;25(4):727–738. doi:10.17305/bb.2024.11280
2. Yi C, Huang S, Zhang W, et al. Synergistic interactions between gut microbiota and short chain fatty acids: pioneering therapeutic frontiers in chronic disease management. *Microb Pathog*. 2025;199:107231. doi:10.1016/j.micpath.2024.107231
3. Liang D, Zhao S, Yin G. Dietary supplementation with soluble corn fiber improved fecal score, microbiota, and SCFAs in dogs. *Front Vet Sci*. 2025;12:1599213. doi:10.3389/fvets.2025.1599213
4. Martin-Gallausiaux C, Marinelli L, Blottière HM, et al. SCFA: mechanisms and functional importance in the gut. *Proc Nutr Soc*. 2021;80(1):37–49. doi:10.1017/S0029665120006916
5. Wang LY, He LH, Xu LJ, et al. Short-chain fatty acids: bridges between diet, gut microbiota, and health. *J Gastroenterol Hepatol*. 2024;39 (9):1728–1736. doi:10.1111/jgh.16619
6. Ma B, Barathan M, Ng MH, et al. Oxidative stress, gut microbiota, and extracellular vesicles: interconnected pathways and therapeutic potentials. *Int J Mol Sci*. 2025;26(7):3148. doi:10.3390/ijms26073148
7. Cheng J, Sui Y, Wang X, et al. Systemic oxidative stress and oxidized albumin mediate the pathogenic kidney-to-gut crosstalk by disrupting intestinal barrier integrity. *Biomolecules*. 2026;16(3):462. doi:10.3390/biom16030462
8. Jouriani FH, Rezaie N, Ashrafian F, et al. Native potential probiotics and postbiotics improve the gut-kidney axis by the modulation of autophagy signaling pathway. *Folia Microbiol*. 2025;12:1–9. doi:10.1007/s12223-025-01253-9
9. Song Y, Chen J, Peng Y, et al. The gut-kidney axis in urolithiasis: extending microbiome research beyond correlation to mechanism. *Urolithiasis*. 2025;53(1):140. doi:10.1007/s00240-025-01811-3
10. Dikalova AE, Itani HA, Nazarewicz RR, et al. Sirt3 impairment and SOD2 hyperacetylation in vascular oxidative stress and hypertension. *Circ Res*. 2017;121(5):564–574. doi:10.1161/CIRCRESAHA.117.310933
11. Winnik S, Auwerx J, Sinclair DA, et al. Protective effects of sirtuins in cardiovascular diseases: from bench to bedside. *Eur Heart J*. 2015;36 (48):3404–3412. doi:10.1093/eurheartj/ehv290
12. Dong X, He Y, Ye F, et al. Vitamin D3 ameliorates nitrogen mustard-induced cutaneous inflammation by inactivating the NLRP3 inflammasome through the SIRT3-SOD2-mtROS signaling pathway. *Clin Transl Med*. 2021;11(2):e312. doi:10.1002/ctm2.312
13. Harijith A, Ebenezer DL, Natarajan V. Reactive oxygen species at the crossroads of inflammasome and inflammation. *Front Physiol*. 2014;5:352. doi:10.3389/fphys.2014.00352
14. Jing E, Emanuelli B, Hirschey MD, et al. Sirtuin-3 (Sirt3) regulates skeletal muscle metabolism and insulin signaling via altered mitochondrial oxidation and reactive oxygen species production. *Proc Natl Acad Sci U S A*. 2011;108(35):14608–14613. doi:10.1073/pnas.1111308108
15. Morigi M, Perico L, Rota C, et al. Sirtuin 3-dependent mitochondrial dynamic improvements protect against acute kidney injury. *J Clin Invest*. 2015;125(2):715–726. doi:10.1172/JCI77632

16. Zhang Y, Wang XL, Zhou M, et al. Crosstalk between gut microbiota and Sirtuin-3 in colonic inflammation and tumorigenesis. *Exp Mol Med*. 2018;50(4):1–11. doi:10.1038/s12276-017-0002-0
17. Xie Z, Zhang M, Luo Y, et al. Healthy human fecal microbiota transplantation into mice attenuates MPTP-induced neurotoxicity via AMPK/SOD2 pathway. *Aging Dis*. 2023;14(6):2193–2214. doi:10.14336/AD.2023.0309
18. Singh V, Ahlawat S, Mohan H, et al. Balancing reactive oxygen species generation by rebooting gut microbiota. *J Appl Microbiol*. 2022;132 (6):4112–4129. doi:10.1111/jam.15504
19. Shen J, Fang L, Wu Y, et al. Intestinal microbiota dysbiosis disrupts the mucosal barrier, triggering inflammatory responses in gut-kidney interaction and exacerbating diarrhea. *J Inflamm Res*. 2025;18:9379–9399. doi:10.2147/JIR.S529493
20. Wu Y, Peng X, Li X, et al. Sex hormones influence the intestinal microbiota composition in mice. *Front Microbiol*. 2022;13:964847. doi:10.3389/fmicb.2022.964847
21. Fang L, Shen J, Wu Y, et al. Involvement of intestinal mucosal microbiota in adenine-induced liver function injury. *3 Biotech*. 2025;15(1):6. doi:10.1007/s13205-024-04180-7
22. Li X, Zhu J, Wu Y, et al. Correlation between kidney function and intestinal biological characteristics of adenine and folium sennaeinduced diarrhea model in mice. *Turk J Gastroenterol*. 2023;34(1):4–12. doi:10.5152/tjg.2022.211010
23. Guo M, Wu Y, Peng M, et al. Decreasing of Trimethylamine N-Oxide by cecal microbiota and choline-trimethylamine lyase are associated with sishen pill on diarrhea with kidney-yang deficiency syndrome. *J Inflamm Res*. 2024;17:7275–7294. doi:10.2147/JIR.S470254
24. Yi X, Zhou K, Deng N, et al. Simo decoction curing spleen deficiency constipation was associated with brain-bacteria-gut axis by intestinal mucosal microbiota. *Front Microbiol*. 2023;14:1090302. doi:10.3389/fmicb.2023.1090302
25. Peng H, Peng X, Liu Q, et al. Novel insights into diarrhea mechanism from gut-kidney axis perspective: correlations among intestinal mucosal injury, AQP4 water transport disorder and gut microbiota dysbiosis. *3 Biotech*. 2026;16(4). doi:10.1007/s13205-026-04774-3
26. Shen J, Fang L, Tan Z, et al. The effects of functional biscuits on intestinal mucosal microbiota composition, brain function, and antioxidant activity. *Biosci Microbiota Food Health*. 2025;44(2):171–181. doi:10.12938/bmfh.2024-078
27. Shen J, Wu Y, Fang L, et al. Huoxiang Zhengqi decoction ameliorates gastrointestinal disorders induced by cold and humid environmental stress via modulation of intestinal mucosal microbiota and amino acid metabolism. *3 Biotech*. 2025;15(6):150. doi:10.1007/s13205-025-04324-3
28. He L, Long C, Liu Y, et al. Effects of *Debaryomyces hansenii* treatment on intestinal microorganisms in mice with antibiotics-induced diarrhea. *3 Biotech*. 2017;7(5):347. doi:10.1007/s13205-017-0953-9
29. Long C, Liu Y, He L, et al. Bacterial lactase genes diversity in intestinal mucosa of dysbacterial diarrhea mice treated with Qiweibaizhu powder. *3 Biotech*. 2018;8(10):423. doi:10.1007/s13205-018-1460-3
30. Shen J, Zhou M, Xiao N, et al. Unveiling the mystery of the stimulatory effects of arecoline: its relevance to the regulation of neurotransmitters and the microecosystem in multi-ecological intestinal sites. *Int J Mol Sci*. 2025;26(7):3150. doi:10.3390/ijms26073150
31. Lin C-H, Jiang W-P, Itokazu N, et al. Chlorogenic acid attenuates 5-fluorouracil-induced intestinal mucositis in mice through SIRT1 signaling-mediated oxidative stress and inflammatory pathways. *Biomed Pharmacother*. 2025;186:117982. doi:10.1016/j.biopha.2025.117982
32. Deng B, Wang K, He H, et al. Biochanin A mitigates colitis by inhibiting ferroptosis-mediated intestinal barrier dysfunction, oxidative stress, and inflammation via the JAK2/STAT3 signaling pathway. *Phytomedicine*. 2025;141:156699. doi:10.1016/j.phymed.2025.156699
33. Guo M, Fang L, Chen M, et al. Dysfunction of cecal microbiota and CutC activity in mice mediating diarrhea with kidney-yang deficiency syndrome. *Front Microbiol*. 2024;15:1354823. doi:10.3389/fmicb.2024.1354823
34. Fu W, Huang Z, Li W, et al. Copper-luteolin nanocomplexes for Mediating multifaceted regulation of oxidative stress, intestinal barrier, and gut microbiota in inflammatory bowel disease. *Bioact Mater*. 2024;46:118–133. doi:10.1016/j.bioactmat.2024.12.004
35. Minutoli L, Puzzolo D, Rinaldi M, et al. ROS-mediated NLRP3 inflammasome activation in brain, heart, kidney, and testis Ischemia/Reperfusion injury. *Oxid Med Cell Longev*. 2016;2016(1):2183026. doi:10.1155/2016/2183026
36. Abais JM, Xia M, Zhang Y, et al. Redox regulation of NLRP3 inflammasomes: ROS as trigger or effector? *Antioxid Redox Signal*. 2015;22 (13):1111–1129. doi:10.1089/ars.2014.5994
37. Hewitt OH, Degnan SM. Antioxidant enzymes that target hydrogen peroxide are conserved across the animal kingdom, from sponges to mammals. *Sci Rep*. 2023;13(1):2510. doi:10.1038/s41598-023-29304-6
38. Grüning NM, Ralser M. Monogenic disorders of ROS production and the primary anti-oxidative defense. *Biomolecules*. 2024;14(2):206. doi:10.3390/biom14020206
39. Khan MA, Younus H. Superoxide dismutase glycation: a contributor to disease and target for prevention. *Catalysts*. 2025;15(3):247. doi:10.3390/catal15030247
40. Yang L, Li Q, Wang S, et al. Sirtuin 3-activated superoxide dismutase 2 mediates fluoride-induced osteoblastic differentiation in vitro and in vivo by down-regulating reactive oxygen species. *Arch Toxicol*. 2024;98(10):3351–3363. doi:10.1007/s00204-024-03819-x
41. Xiao Y, Feng Y, Zhao J, et al. Achieving healthy aging through gut microbiota-directed dietary intervention: focusing on microbial biomarkers and host mechanisms. *J Adv Res*. 2025;68:179–200. doi:10.1016/j.jare.2024.03.005
42. Leao L, Miri S, Hammami R. Gut feeling: exploring the intertwined trilateral nexus of gut microbiota, sex hormones, and mental health. *Front Neuroendocrinol*. 2025;76:101173. doi:10.1016/j.yfrne.2024.101173
43. Perrone P, D'Angelo S. Gut microbiota modulation through mediterranean diet foods: implications for human health. *Nutrients*. 2025;17(6):948. doi:10.3390/nu17060948
44. Beaver LM, Jamieson PE, Wong CP, et al. Promotion of healthy aging through the nexus of gut microbiota and dietary phytochemicals. *Adv Nutr*. 2025;16(3):100376. doi:10.1016/j.advnut.2025.100376
45. Kumar S, Mukherjee R, Gaur P, et al. Unveiling roles of beneficial gut bacteria and optimal diets for health. *Front Microbiol*. 2025;16:1527755. doi:10.3389/fmicb.2025.1527755
46. Shao H, Zhang C, Wang C, et al. Intestinal mucosal bacterial diversity of antibiotic-associated diarrhea (AAD) mice treated with *Debaryomyces hansenii* and Qiweibaizhu powder. *3 Biotech*. 2020;10(9):392. doi:10.1007/s13205-020-02383-2
47. Hu C, Rzymski P. Non-photosynthetic melainabacteria (Cyanobacteria) in human gut: characteristics and association with health. *Life*. 2022;12 (4):476. doi:10.3390/life12040476
48. Zhang T, Liu D, Zhang Y, et al. Biomedical engineering utilizing living photosynthetic cyanobacteria and microalgae: current status and future prospects. *Mater Today Bio*. 2024;27:101154. doi:10.1016/j.mtbio.2024.101154

49. Bouyahya A, Bakrim S, Chamkhi I, et al. Bioactive substances of cyanobacteria and microalgae: sources, metabolism, and anticancer mechanism insights. *Biomed Pharmacother*. 2024;170:115989. doi:10.1016/j.biopha.2023.115989
50. Zahra Z, Choo DH, Lee H, et al. Cyanobacteria: review of current potentials and applications. *Environments*. 2020;7(2):13. doi:10.3390/environments7020013
51. Nawaz T, Gu L, Fahad S, et al. Unveiling the antioxidant capacity of fermented foods and food microorganisms: a focus on cyanobacteria. *J Umm Al-Qura Univ Appll Sci*. 2024;10:232–243. doi:10.1007/s43994-023-00095-w
52. Rodrigues F, Reis M, Ferreira L, et al. The neuroprotective role of cyanobacteria with focus on the anti-inflammatory and antioxidant potential: current status and perspectives. *Molecules*. 2024;29(20):4799. doi:10.3390/molecules29204799
53. Lannes-Costa PS, de Oliveira JSS, da Silva Santos G, et al. A current review of pathogenicity determinants of Streptococcus sp. *J Appl Microbiol*. 2021;131(4):1600–1620. doi:10.1111/jam.15090
54. Yang J, Ma Y, Tan Q, et al. Gut *Streptococcus* is a microbial marker for the occurrence and liver metastasis of pancreatic cancer. *Front Microbiol*. 2023;14:1184869. doi:10.3389/fmicb.2023.1184869
55. Ohashi A, Murayama MA, Miyabe Y, et al. Streptococcal infection and autoimmune diseases. *Front Immunol*. 2024;15:1361123. doi:10.3389/fimmu.2024.1361123
56. Wang Y, Wang Y, Han W, et al. Intratumoral and fecal microbiota reveals microbial markers associated with gastric carcinogenesis. *Front Cell Infect Microbiol*. 2024;14:1397466. doi:10.3389/fcimb.2024.1397466
57. Krzyściak W, Pluskwa KK, Jurczak A, et al. The pathogenicity of the Streptococcus genus. *Eur J Clin Microbiol Infect Dis*. 2013;32(11):1361–1376. doi:10.1007/s10096-013-1914-9
58. Dąbek-Drobny A, Kaczmarczyk O, Woźniakiewicz M, et al. Association between fecal short-chain fatty acid levels, diet, and body mass index in patients with inflammatory bowel disease. *Biology*. 2022;11(1):108. doi:10.3390/biology11010108
59. Bikbavova GR, Livzan MA, Lisyutenko NS, et al. Cardiovascular risks in patients with ulcerative colitis: the role of assessing the markers of systemic inflammation and metabolic activity of intestinal microbiota. *Therapy*. 2025;11(5):17–25. doi:10.18565/therapy.2025.5.17-25
60. Liu XC, Du TT, Gao X, et al. Gut microbiota and short-chain fatty acids may be new biomarkers for predicting neonatal necrotizing enterocolitis: a pilot study. *Front Microbiol*. 2022;13:969656. doi:10.3389/fmicb.2022.969656
61. Facchin S, Calgaro M, Savarino EV. Rethinking short-chain fatty acids: a closer look at propionate in inflammation, metabolism, and mucosal homeostasis. *Cells*. 2025;14(15):1130. doi:10.3390/cells14151130
62. Nastasi C, Fredholm S, Willerslev-Olsen A, et al. Butyrate and propionate inhibit antigen-specific $CD8^+$ T cell activation by suppressing IL-12 production by antigen-presenting cells. *Sci Rep*. 2017;7(1):14516. doi:10.1038/s41598-017-15099-w
63. He KY, Lei XY, Wu DH, et al. Akkermansia muciniphila protects the intestine from irradiation-induced injury by secretion of propionic acid. *Gut Microbes*. 2023;15(2):2293312. doi:10.1080/19490976.2023.2293312
64. Wang B, Hou J, Cao Y, et al. Dietary isobutyric acid supplementation improves intestinal mucosal barrier function and meat quality by regulating cecal microbiota and serum metabolites in weaned piglets. *Front Vet Sci*. 2025;12:1565216. doi:10.3389/fvets.2025.1565216